

ELECTRONIC AND THERMOELECTRIC PROPERTIES OF PURE AND ALLOYS In_2O_3 TRANSPARENT CONDUCTORS

S. M. HOSSEINI*, H. A. RAHNAMAYE ALIABAD and A. KOMPANY

*Department of Physics (Materials and Electroceramics Laboratory),
Ferdowsi University of Mashhad, Iran*

**seyedhosseini@um.ac.ir*

Received 2 September 2009

Revised 4 January 2010

Electronic and thermoelectric properties of pure In_2O_3 and $\text{In}_{1.5}\text{T}_{0.5}\text{O}_3$ ($T = \text{Sc}, \text{Y}$) alloys including the band gap, the electrical and thermal conductivity, Seebeck coefficient and figure of merit have been investigated using semi-classical Boltzmann transport theory. The calculated results indicated that substituting indium atoms by these dopants have a significant influence on the electronic properties of alloyed In_2O_3 crystals. Substitution of Sc and Y atoms for In atoms increases the band gaps and Seebeck coefficient. The intrinsic relations between electronic structures and the transport performances of In_2O_3 and its alloys with Sc and Y are also discussed.

Keywords: Density functional theory; thermoelectric effects; transport coefficients; effective mass.

PACS Number(s): 71.15.Mb, 72.15.Jf, 72.10.Bg, 71.18.+y

1. Introduction

Thermoelectric materials have been used as sensors a long time. One of the most reliable ways to measure temperature is by thermocouples. Several new principles, using thermoelectric materials for measuring other parameters such as gas sensor,¹ humidity,² chemical species,³ flow velocity^{4,5} and other biochemical parameters have been reported and incorporated into MEMS (micro electro-mechanical systems).^{6,7} The Seebeck effect lends itself to such an implantation and examples of chemical sensors based upon the change of the Fermi level with chemisorptions.

Over the last two decades, there has been increasing attention in both fundamental research and industrial applications of transparent conducting oxides (TCOs). These materials have many applications in numerous devices such as flat panel displays, solar cells, gas sensors and low-emissive windows.^{8,9} Among the various transparent oxides indium tin oxide (ITO), indium oxide (In_2O_3), tin oxide (SnO_2), and zinc oxide (ZnO) are the dominant TCOs. Tin-doped indium oxide, with a typical electrical conductivity and transparency in the visible region is usually used

*Corresponding author.

in thin-coating form. The development of polycrystalline or amorphous transparent conducting oxide semiconductors used for practical thin-film transparent electrode applications has also been discussed widely in literature during the last few years.^{10,11}

There is a possibility to control the electronic and thermoelectric properties of In_2O_3 with the transition metal doping, since the d states of these metals are very sensitive. Substituting indium atoms at b positions (see Fig. 1) by IIIB elements considerably increases the value of the band gap mainly due to number of states originating from IIIB- d states in the conduction bands.^{12–14} Medvedeva¹⁵ have demonstrated that doping In_2O_3 with the transition metal (Mo) results in a smaller effective mass, larger fundamental band gap, and overall optical better transmission in the visible region as compared to commercial Sn-doped In_2O_3 .

The mobility of transparent oxides materials are high and therefore has had great interest in exploring In_2O_3 as an excellent candidate for thermoelectric materials with high figures of merit.¹⁶

However, the theoretical aspects of thermoelectric properties of pure and doped In_2O_3 have rarely been studied, and a few experimental articles on series of complex oxide In_2O_3 at high temperature have been published.^{17–20} De Wit *et al.*²¹ have measured and reported the Seebeck coefficient of pure In_2O_3 from room temperature to 700°C. Thermoelectric properties of air-prepared co-substituted indium oxide based compounds belonging to the series $\text{In}_{2-2x}\text{M}_x\text{Sn}_x\text{O}_3$ ($\text{M} = \text{Zn}, \text{Cu}, \text{or Ni}$) have been studied by Bérardan *et al.*¹⁶ Their experimental published data have indicated that the thermoelectric power factor is significantly higher than undoped In_2O_3 .

Moreover, it is well-known that the efficiency of a thermoelectric material is given by the dimensionless figure of merit $TZ = (\sigma TS^2)/\kappa$, where S is the Seebeck coefficient, σ is the electrical and κ is the thermal conductivity, respectively. The electronic structure near the Fermi level of a semiconductor can give much information about the physical quantities such as S, σ, κ and also determines their thermoelectric properties. For this reason, in this work, first we have calculated the electronic properties and obtained the band structure data. Then from semi-classical Boltzmann transport theory, thermal conductivity, Seebeck coefficient and figure of merit, we evaluated via first principle calculations.

2. Method of Calculations

The calculations of band structure were carried out with a self-consistent scheme by solving the Kohn–Sham equations using a FP-LAPW method in the framework of DFT along with the local density approximation,^{22,23} using Wien2k codes.²⁴ The calculation was performed with 24000 k -points and $Rk_{\text{max}} = 6$ (R is the smallest muffin-tin radius and k_{max} is the cut-off for the plane wave) for the convergence parameter in which the calculations stabilize and converge in terms of the desired charge e.g. less than 0.001e between steps. The values of the other parameters are

$G_{\max} = 12$ (magnitude of largest vector in charge density Fourier expansion or the plane wave cut-off), the muffin-tin radii for In and O $R_{MT}(\text{In}) = 2.0$ au and $R_{MT}(\text{O}) = 1.6$ au, respectively. The cut-off energy, which defines the separation of the valence and core states, was chosen to be -7 Ry.

After obtaining the band structure data, we fitted them into a semi-classical Boltzmann package²⁵ in order to obtain the thermoelectric properties of pure and doped In_2O_3 . In this package, the transport coefficients were based on the rigid band approach to conductivity as follows:

$$\sigma_{\alpha\beta} = \frac{1}{N} \sum_{i,\mathbf{k}} \sigma_{\alpha\beta}(i, \mathbf{k}) \frac{\delta(\varepsilon - \varepsilon_{i,\mathbf{k}})}{d\varepsilon}, \quad (1)$$

where N is the number of \mathbf{k} -points sampled. The \mathbf{k} -dependent transport tensor is given by

$$\sigma_{\alpha\beta}(i, \mathbf{k}) = e^2 \tau_{i,\mathbf{k}} v_{\alpha}(i, \mathbf{k}) v_{\beta}(i, \mathbf{k}), \quad (2)$$

where τ is the relaxation time and $v_{\alpha}(i, \mathbf{k})$ is a component of the group velocities. The transport coefficients can be calculated as a function of temperature, T , and chemical potential, μ , by integrating the transport distribution^{25,26}

$$\sigma_{\alpha\beta}(T; \mu) = \frac{1}{\Omega} \int \sigma_{\alpha\beta}(\varepsilon) \left[-\frac{\partial f_{\mu}(T; \varepsilon)}{\partial \varepsilon} \right] d\varepsilon \quad (3)$$

$$v_{\alpha\beta} = (T; \mu) = \frac{1}{eT\Omega} \int \sigma_{\alpha\beta}(\varepsilon) (\varepsilon - \mu) \left[-\frac{\partial f_{\mu}(T; \varepsilon)}{\partial \varepsilon} \right] d\varepsilon, \quad (4)$$

where f is the Fermi–Dirac distribution function. In this approach, the chemical potential μ determines the number of carriers and assumes the shape of band structure, and hence $\sigma(\varepsilon)$ are left fixed (i.e. rigid band approach) for each component. By moving the Fermi-level up or down, we can simulate n - or p -doped environment. This approximation is good as long as the doping levels used are not high enough to modify the bonding properties of the material. This means, only one band structure calculation needs to be performed per compound. Otherwise, every time we simulated the compound for n or p -doped, a new band structure must be calculated.

In the calculations of transport coefficients, the relaxation time τ is a necessary input. In the present work, we treat it as a constant. With this simplification, one can calculate the Seebeck coefficient $S = \sigma^{-1}$ having only the band structure information, independent of τ . However, the electronic conductivity can only be calculated with respect to the relaxation time.

3. Results and Discussion

3.1. Structure

Indium oxide can exist in three different phases²⁷ characterized by space group symmetries $I2_13$, $Ia\bar{3}$ and $R\bar{3}$. In_2O_3 with space group $Ia\bar{3}$ and the band gap of

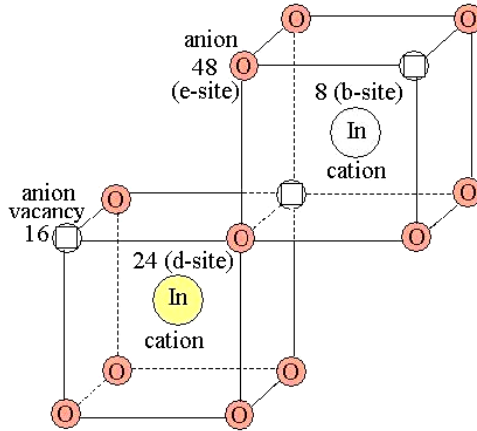


Fig. 1. Non-equivalent cation sites and anion vacancies in In_2O_3 .

$E_g = 3.7$ eV is similar to many trivalent rare-earth oxides, such as Yb_2O_3 and Dy_2O_3 . This phase of indium oxide has two non-equivalent six-fold coordinated cation sites, as shown in Fig. 1.

The two cations sites referred as equipoints “*b*” and “*d*”. The *b* site cations have six equidistant oxygen anion neighbors, which lie approximately at the corners of a cube with two anion structural vacancies along one body diagonal.²⁸ In this paper, the *b* and *d* site cations referred as cation I, II with (8a), (24d) Wyckoff positions, respectively, and oxygen’s with (48e) Wyckoff positions.

The sites of the cations are coordinated to six oxygen anions at three different distances, which lie near the corners of a distorted cube with two empty ions along one face diagonal. The unit cell containing 80 atoms and crystallized in cubic bixbyite structure. The actual unit cell is body-centered and contains eight formula units of In_2O_3 with eight indium atoms at *b* positions, 24 atoms at *d* and 48 oxygen atoms at *e* positions.

The calculations were first carried out by applying the experimental data for the lattice constants. Then by minimizing the total energy of the crystal to the volume, the theoretical lattice constants were obtained. We substituted the impurities in *b* positions, since at low temperatures the impurities prefer to sit at *b* positions.²⁹ For simplicity, we assumed that doping In_2O_3 with Sc and Y does not change the symmetries of the crystal and we have again the lattice with the same space group ($Ia\bar{3}$). We minimized the energy for atomic positions and determined the equilibrium position of individual atoms. The final calculations were performed with the theoretical lattice constant and relaxed structure.

Table 1 lists the full relaxation of anion positions for alloyed $\text{In}_{1.5}\text{T}_{0.5}\text{O}_3$. From this table, it can be seen that the lattice parameters of $\text{In}_{1.5}\text{Sc}_{0.5}\text{O}_3$ are smaller than In_2O_3 due to smaller ionic size of Sc (0.745 Å), comparing to In (0.8 Å), while Y (0.9 Å), with larger ionic size causes the expansion of the In_2O_3 lattice.

Table 1. Calculated lattice parameter and Wyckoff positions for $\text{In}_{1.5}\text{T}_{0.5}\text{O}_3$ (T = Sc, Y).

	In_2O_3 This work	In_2O_3 Experimental ³⁰ (Neutron diffraction)	$\text{In}_{1.5}\text{Sc}_{0.5}\text{O}_3$	$\text{In}_{1.5}\text{Y}_{0.5}\text{O}_3$
Lattice parameter (Å)	10.057	10.121	9.987	10.187
Cation I (8b)				
<i>x</i>	0.25	0.25	0.25	0.25
<i>y</i>	0.25	0.25	0.25	0.25
<i>z</i>	0.25	0.25	0.25	0.25
Cation II (24d)				
<i>x</i>	0.4659	0.4660	0.4653	0.4668
<i>y</i>	0.0000	0.0000	0.0000	0.0000
<i>z</i>	0.2500	0.2500	0.2500	0.2500
O (48e)				
<i>x</i>	0.3899	0.3900	0.3876	0.3929
<i>y</i>	0.1543	0.1550	0.1580	0.1522
<i>z</i>	0.3821	0.3820	0.3811	0.3843

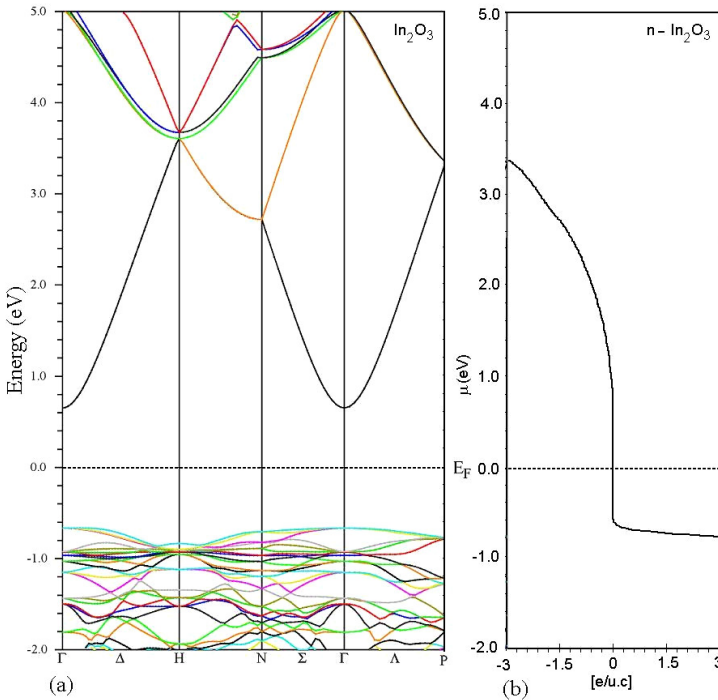


Fig. 2. (a) Calculated band structures and (b) number of carrier for pure In_2O_3 in the primitive Brillouin zone.

3.2. The band structure and density of states

We have calculated the value of the band gaps of pure In_2O_3 and alloyed $\text{In}_{1.5}\text{T}_{0.5}\text{O}_3$ from the band structure as shown in Figs. 2–4 using GGA approach. The overall

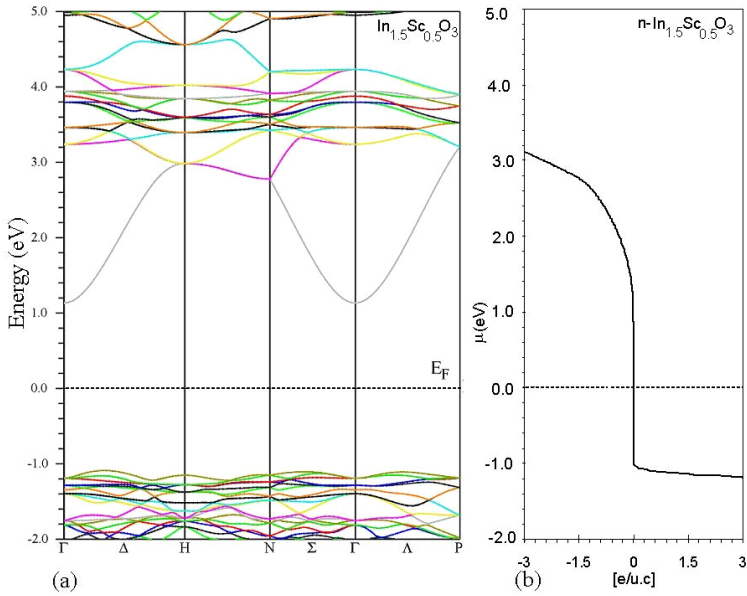


Fig. 3. (a) Calculated band structures and (b) number of carrier for $\text{In}_{1.5}\text{Sc}_{0.5}\text{O}_3$ in the primitive Brillouin zone.

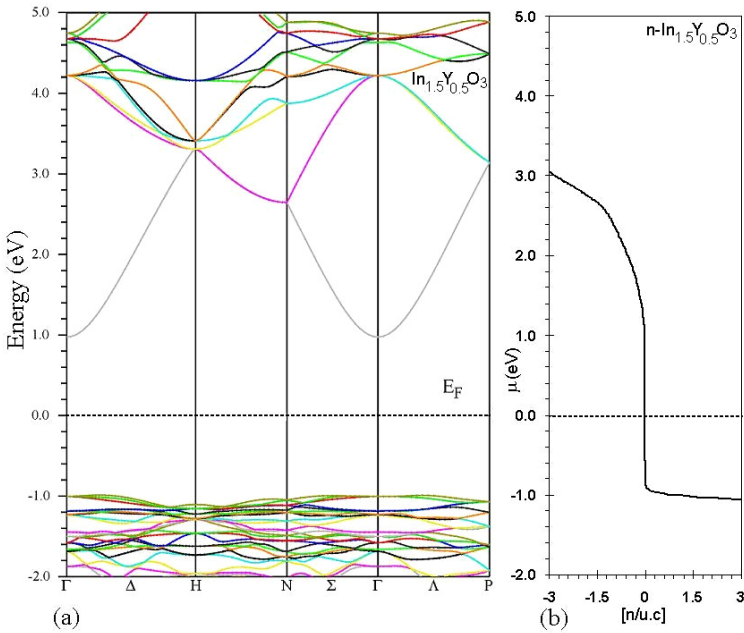


Fig. 4. (a) Calculated band structures and (b) number of carrier for $\text{In}_{1.5}\text{Y}_{0.5}\text{O}_3$ in the primitive Brillouin zone.

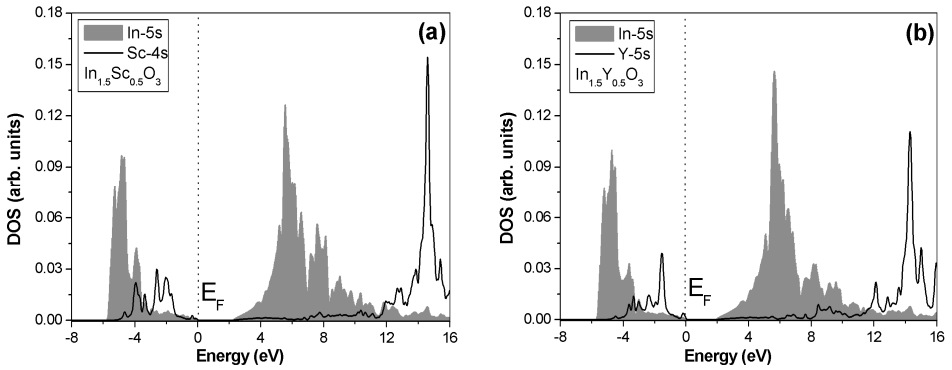


Fig. 5. Calculated partial density of states for (a) In 5s and Sc 4s in $\text{In}_{1.5}\text{Sc}_{0.5}\text{O}_3$, (b) In 5s and Y 5s in $\text{In}_{1.5}\text{Y}_{0.5}\text{O}_3$.

band profiles calculated in this work are consistent with other first-principles calculation results reported previously.^{26,31–33} The scale of energy in all figures is in eV and the middle of the band gap is set to zero (as arbitrary Fermi level) on the energy scale. The valence bands are separated by 1.28 eV energy gap directly from the conduction band states at Γ point. Experimental value of In_2O_3 band gap is about 3.6 eV at Γ point and is a direct band gap.³⁴ Our calculated band gap is smaller than the experimental value. This discrepancy mainly arises from the DFT approximation, which is known to underestimate the energy band gap of semiconductors and insulators. The bottom of conduction band is almost parabolic, while for the valence band is flat. In Figs. 2–4 in addition to band structure, the calculated number of carriers n (density of states) as function of chemical energy are shown.

The calculated energy gaps for In_2O_3 , $\text{In}_{1.5}\text{Sc}_{0.5}\text{O}_3$ and $\text{In}_{1.5}\text{Y}_{0.5}\text{O}_3$ are 1.28, 2.20, 1.90 eV respectively which indicate that the substitution of Sc and Y atoms for In have increased the band gaps of the doped In_2O_3 . However, replacement of Sc and Y causes the rise of band gap mainly due to many body effects.

In Fig. 5, the partial DOS is shown for the alloyed In_2O_3 as a function of energy. The main contribution to the bottom of the conduction band (CB) is mainly composed of In-5s and Sc-4s and Y-5s orbitals with small hybridization between them. As the electronic charge density of s -type orbital in the bottom of the conduction band is a uniform distribution, therefore it has relatively low scattering. The high dispersion and s -type character orbitals indicate the high conductivity and hence as a result of high mobility of these states.

3.3. Electrical conductivity

The electrical conductivity, σ can be calculated with respect to the relaxation time, τ , from Eq. (1) which is somehow included as a parameter. The number of carrier's concentration changes by varying the chemical potential and temperature. The

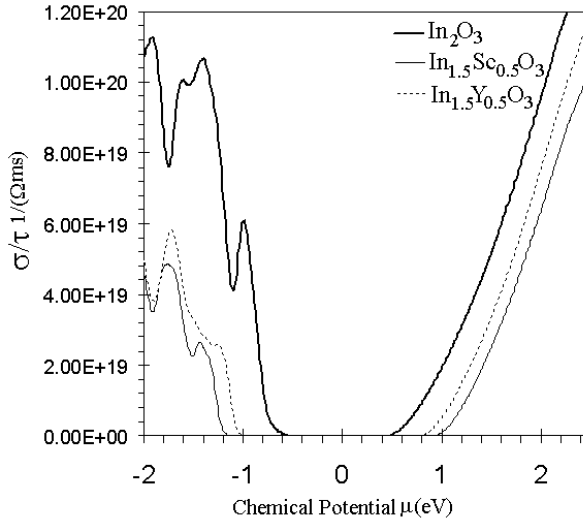


Fig. 6. The conductivity as a function of chemical potential at 300 K for pure and alloy In_2O_3 .

calculation of conductivity was performed at $T = 300$ K and this is illustrated in Fig. 6 as a function of chemical potential for pure and alloyed In_2O_3 .

The conductivity of pure In_2O_3 is larger, comparing to alloy In_2O_3 , due to the smaller value of the band gap. When the chemical potential is zero or the Fermi level is exactly in the middle of the band structure, these components have insulator behavior. Increasing the chemical potential or moving the Fermi level toward the conduction band system causes the behavior to be as n -type semiconductor and moving downward to the valence band causes the behavior to be as p -type semiconductor.

3.4. Seebeck coefficient

If the temperature differences exist between different material, then the thermoelectric voltages is induced across material. In the Seebeck effect, the temperature difference produces a voltage of several microvolts per Kelvin between two materials.

The Seebeck coefficient has the units of (V/K). Doped semiconductors can have a large Seebeck coefficient, depending on the excess charge carriers. The sign of the thermopower can determine which charged carriers dominate the electric transport in the material. The Seebeck coefficient can be calculated from the following relation²⁵

$$S_{ij} = -(\Delta V/\Delta T) = E_i(\nabla_j T)^{-1} = (\sigma^{-1})_{\alpha i} v_{\alpha j}. \quad (5)$$

A larger induced thermoelectric voltage, for a given temperature gradient, will lead to a higher efficiency. Ideally, one would like very large thermopower values since only a small amount of heat is then necessary to create a large voltage.

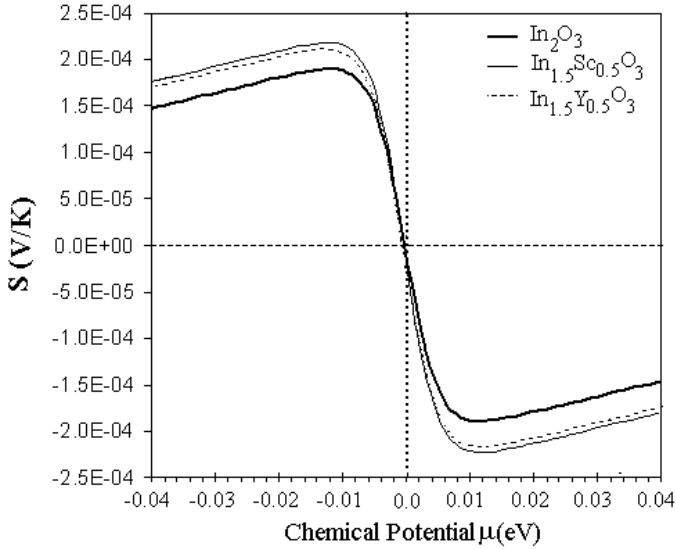


Fig. 7. Seebeck coefficient as function of chemical potential for pure and alloy In_2O_3 .

It is clear that a good thermoelectric material should have high electrical conductivity to minimize the Joule heating, low thermal conductivity to prevent thermal shorting, and high Seebeck coefficient for maximum conversion of heat to electrical power or electrical power to cooling performance. The Seebeck coefficient as function of chemical potential at 300 K for pure and alloyed In_2O_3 is shown in Fig. 7.

The thermoelectric values are positive when the Fermi level shift down toward to the valence band indicating *p*-type conduction and the Seebeck coefficients are negative when the Fermi level shift upward to the conduction band indicating *n*-type conduction, at room temperature.

The Seebeck coefficient is lower for pure In_2O_3 and the maximum value is ± 0.190 (mV/K), corresponding to the chemical potential, ∓ 0.012 eV. For doped In_2O_3 , this is significantly higher and leading to the values exceeding ± 0.232 (mV/K) and ± 0.231 (mV/K) with Sc and Y, respectively. The calculated result for pure *n*-type In_2O_3 is close to the reported experimental value ± 0.26 (mV/K).²¹

Keeping τ constant for all doping levels, we calculated the power factor as a function of doping as shown in Fig. 8 for In_2O_3 and alloyed $\text{In}_{1.5}\text{T}_{0.5}\text{O}_3$. The power factor of doping with In_2O_4 with Sc is higher than pure In_2O_4 .

3.5. Thermal conductivity

The thermal conductivity, κ , of a material indicates its ability to conduct heat for both the electronic and lattice contributions. Thus, the total thermal conduc-

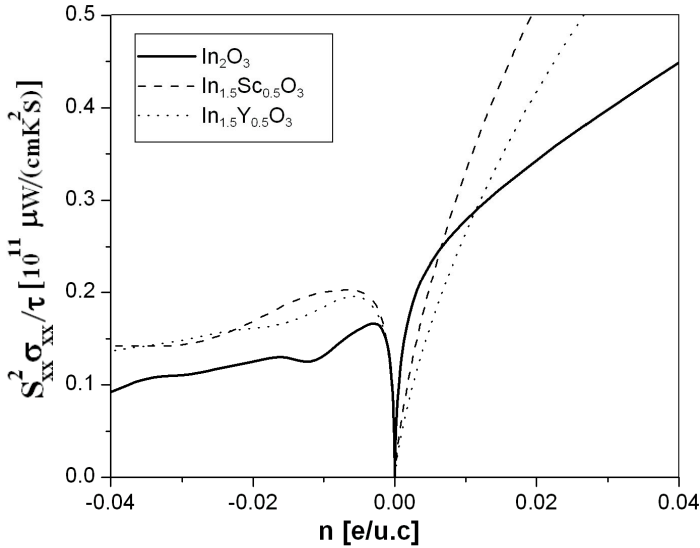


Fig. 8. The power factor with respect to scattering time $s^2\sigma/\tau$ as function of carrier for pure and alloy In_2O_3 .

tivity of a material will be the sum of the electronic thermal conductivity and the corresponding lattice contribution. In doped semiconductors, the thermal conductivity is usually dominated by lattice thermal conductivity, while in metals the electronic term is large and normally dominates according to the Wiedemann–Franz law ($k_{\text{el}} = L_0\sigma T$, where $L_0 = \pi^2/3(k_B/e)^2 = 2.45 \times 10^{-8} \text{ V}^2/\text{K}^2$ is the Lorentz constant). Actually, the lattice thermal conductivity may decrease due to the impurity scattering. In this semi-classical Boltzmann package, the electronic thermal conductivity, κ_{el} , at zero electric current is defined as²⁵

$$\kappa_{\text{el}} = \kappa^0 - T\sigma S^2, \tag{6}$$

where κ^0 is given by

$$\kappa_{\alpha\beta}^0(T; \mu) = \frac{1}{e^2 T \Omega} \int \sigma_{\alpha\beta}(\varepsilon) (\varepsilon - \mu)^2 \left[-\frac{\partial f_u(T; \varepsilon)}{\partial \varepsilon} \right] d\varepsilon. \tag{7}$$

Figure 9 shows the electronic thermal conductivity from Eqs. (5) and (6) as a function of chemical potential for In_2O_3 and alloyed $\text{In}_{1.5}\text{T}_{0.5}\text{O}_3$.

3.6. Effective mass

The Brillouin zone of In_2O_3 with $Ia\bar{3}$ space group (number 206) can be shown by either primitive or conventional as indicated in Fig. 10.²⁷ In this paper, the effective electron mass of In_2O_3 and $\text{In}_{1.5}\text{T}_{0.5}\text{O}_3$ have been calculated for the six directions in the primitive and conventional Brillouin zones.

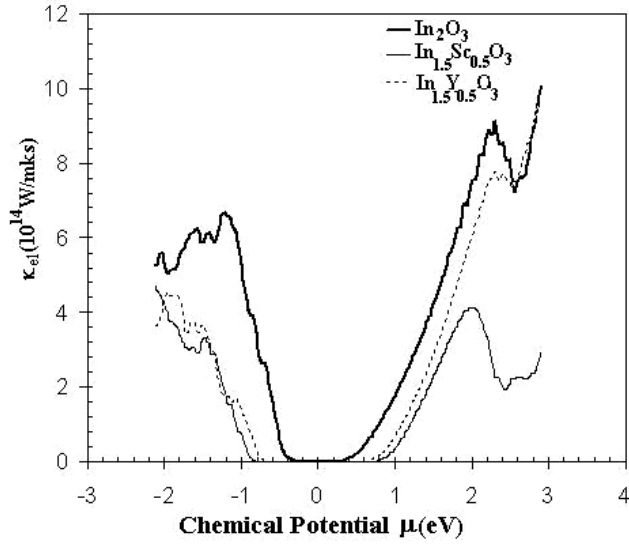


Fig. 9. Electronic thermal conductivity as function of chemical potential for In_2O_3 and alloy $\text{In}_{1.5}\text{T}_{0.5}\text{O}_3$.

These directions of high symmetry are for primitive and conventional Brillouin zones as follows:

Conventional Brillouin zone:

$$\Gamma(0, 0, 0) \rightarrow X(1/2, 0, 0)$$

$$\Gamma(0, 0, 0) \rightarrow M(1/2, 1/2, 0)$$

$$\Gamma(0, 0, 0) \rightarrow R(1/2, 1/2, 1/2).$$

Primitive Brillouin zone:

$$\Gamma(0, 0, 0) \rightarrow H(1/2, -1/2, 1/2)$$

$$\Gamma(0, 0, 0) \rightarrow P(1/4, 1/4, 1/4)$$

$$\Gamma(0, 0, 0) \rightarrow N(0, 0, 1/2).$$

The diagonal elements of the effective mass tensor, m_e^* , for the electrons in the conduction band were calculated in different directions in k -space from the following well-known relation:

$$\frac{1}{m_e^*(k)} = \frac{1}{\hbar^2} \frac{\partial^2 E(k)}{\partial k^2}. \quad (8)$$

The electron effective mass for pure and the alloys of In_2O_3 was obtained from the curvature of the conduction band at Γ point. To illustrate how the alloying by transition metals alters the electronic band structure of the host material, we have enlarged the band structures of pure In_2O_3 and alloyed it with Sc and Y as illustrated in Fig. 11. The bottom of the conduction band structure has been plotted for two directions $\Gamma \rightarrow X$ and $\Gamma \rightarrow H$.

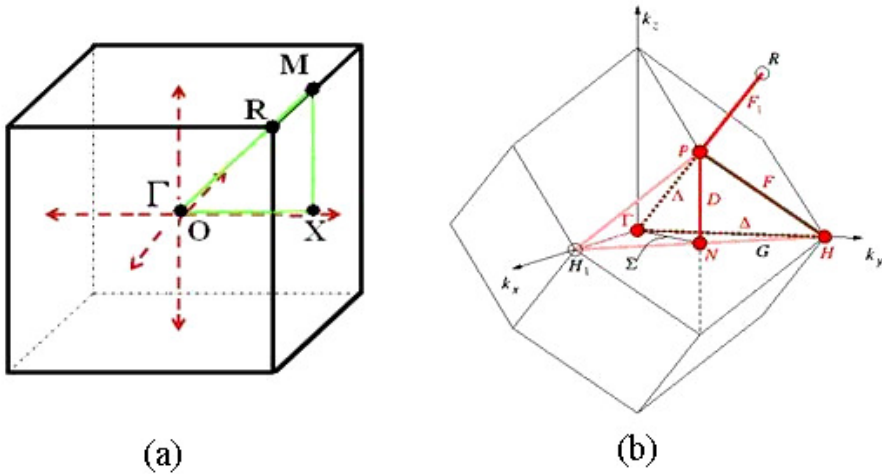


Fig. 10. (a) Conventional and (b) primitive Brillouin zone for In_2O_3 .

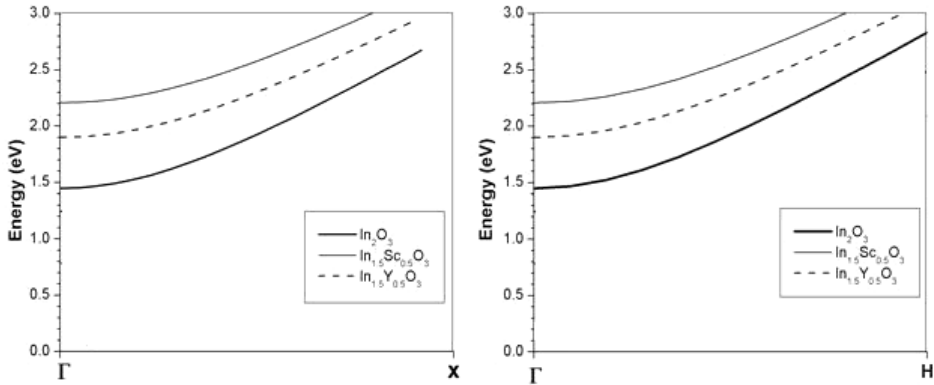


Fig. 11. The calculated bands at the bottom of the conduction band for In_2O_3 , $\text{In}_{1.5}\text{Sc}_{0.5}\text{O}_3$ and $\text{In}_{1.5}\text{Y}_{0.5}\text{O}_3$ (a) $\Gamma \rightarrow X$ (conventional), (b) $\Gamma \rightarrow H$ (primitive) Brillouin zone.

The electron effective mass has been determined from fitting the electronic band structure to a parabolic function (Eq. (8)) for the six directions in the first Brillouin zone. The values of calculated electron effective mass for In_2O_3 in $\Gamma \rightarrow X$, $\Gamma \rightarrow M$ and $\Gamma \rightarrow R$ directions are $0.374m_e$, $0.386m_e$, $0.391m_e$ respectively in the conventional Brillouin zone. Nevertheless, for the $\Gamma \rightarrow H$, $\Gamma \rightarrow P$ and $\Gamma \rightarrow N$ directions in primitive Brillouin zone are $0.400m_e$, $0.391m_e$ and $0.419m_e$ respectively. The corresponding values for pure In_2O_3 , alloys of $\text{In}_{1.5}\text{T}_{0.5}\text{O}_3$, pure Cd_3TeO_6 and doped with In obtained by the others are also summarized in the Table 2.

Table 2. Calculated electron effective mass in the conduction band for In_2O_3 and $\text{In}_{1.5}\text{T}_{0.5}\text{O}_3$ in conventional and primitive Brillouin zone direction.

Brillouin zone directions	Conventional				Primitive	
	$\Gamma \rightarrow X$	$\Gamma \rightarrow M$	$\Gamma \rightarrow R$	$\Gamma \rightarrow H$	$\Gamma \rightarrow P$	$\Gamma \rightarrow N$
This work: (FL-LAPW method GGA)						
In_2O_3	$0.380m_e$	$0.385m_e$	$0.387m_e$	$0.397m_e$	$0.387m_e$	$0.415m_e$
$\text{In}_{1.5}\text{Sc}_{0.5}\text{O}_3$	$0.538m_e$	$0.543m_e$	$0.550m_e$	$0.556m_e$	$0.550m_e$	$0.572m_e$
$\text{In}_{1.5}\text{Y}_{0.5}\text{O}_3$	$0.488m_e$	$0.498m_e$	$0.507m_e$	$0.514m_e$	$0.507m_e$	$0.529m_e$
Theory:						
In_2O_3 (quantum chemical software) DMol3 ³⁵						
	$0.300m_e$	$0.360m_e$	$0.410m_e$	—	—	—
In_2O_3 (GGA) ²⁷	—	—	—	$0.230m_e$	$0.200m_e$	$0.230m_e$
In_2O_3 (tight-binding linear muffin-tin orbital) LMTO method ³²						
	—	—	—	$0.420m_e$	$0.300m_e$	$0.360m_e$
$\text{In}_{30}\text{Sn}_2\text{O}_{48}$ (quantum chemical software) DMol3 ³⁵						
	$0.320m_e$	$0.470m_e$	$0.640m_e$	—	—	—
Cd_3TeO_6 (FLAPW method, GGA) ³⁶						
	$0.206m_e$	$0.210m_e$	$0.214m_e$	—	—	—
Cd_3TeO_6 (FLAPW method, GGA) ^{36*}						
	$0.291m_e$	$0.293m_e$	$0.309m_e$	—	—	—
Experimental:						
Sn doped In_2O_3 (Ref. 37)	—	—	—		$0.300m_e$	
In_2O_3 (thin films) ³⁸	—	—	—		$0.31m_e$ to $0.43m_e$	

* Cd_3TeO_6 substituted with In in B -site.

Note: The ternary oxide Cd_3TeO_6 has a deformed perovskite-type structure, ABO_3 (monoclinic, $P2_1/n$) in which B -sites are occupied by Cd^{2+} and Te^{6+} ions in a ratio of 1:1 and A-sites are filled solely by Cd^{2+} ions.

The value of the electron effective mass in the conduction band is increased in all the six directions for In_2O_3 alloys, so the mobility of electrons is decreased in these directions.

4. Conclusions

In this work, we have studied the thermoelectric properties of In_2O_3 and alloyed $\text{In}_{1.5}\text{T}_{0.5}\text{O}_3$ ($T = \text{Sc}, \text{Y}$). We have considered the effect of dopant on the lattice parameters and Wyckoff positions of the atoms. In addition, the electrical and thermal conductivity, Seebeck coefficient, figure of merit and the effective electron mass in the primitive and conventional Brillouin zone were discussed. Our results show that the Seebeck coefficient is significantly higher than that of the undoped

In_2O_3 . However, to our knowledge, there is no theoretical and experimental results to compare with the results presented in this paper. The electron effective mass in the conduction band has increased along the six directions, resulting in the decrease of the mobility of electrons.

Acknowledgment

This work is supported by the Ferdowsi University of Mashhad (Iran) as a grant project. The authors are grateful to Professor P. Blaha (at Vienna University of Technology Austria) for his technical assistance in using Wien2k codes.

References

1. W. Shin, M. Matsumiya, F. Qiu, N. Izu and N. Murayama, *Sensors and Actuators B* **97** (2004) 344–347.
2. N. Sawaguchi, W. Shin, N. Izu, I. Matsubara and N. Murayama, *Sensors and Actuators B* **108** (2005) 461–466.
3. S. Masubuchi, S. Kazama, K. Mizoguchi, F. Shimizu, K. Kume, R. Matsushita and T. Matsuyama, *Synthetic Metals* **69** (1995) 71–72.
4. A. I. Bannikov, V. A. Khristich and G. N. Lyubchik, *J. Eng. Phys. Thermophys.* **9** (1965) 333–336.
5. H. Stachowiak, S. Lassue, A. Dubernard and E. Gaviot, *Flow Measurement and Instrumentation* **9** (1998) 135–141.
6. S. A. Jacobson and A. H. Epstein, An informal survey of power MEMS, *Int. Symp. Micro-Mechanical Engineering (ISMME2003-K18)*, 1–3 December (2003).
7. J. W. Judy, *Smart Mater. Struct.* **10** (2001) 1115–1134.
8. T. J. Coutts, J. D. Perkins, D. S. Ginley and T. O. Mason, Transparent conducting oxides: Status and opportunities in basic research, in *195th Meeting of the Electrochemical Society*, Seattle, Washington, 2–6 May (1999).
9. D. S. Ginley and C. Bright (eds.), *Transparent Conducting Oxides*, MRS Bulletin, 15–18 August (2000) www.mrs.org/publications/bulletin.
10. T. Minami, *Semicond. Sci. Technol.* **20** (2005) S35.
11. N. G. Lewis and D. C. Paine, *MRS Bulletin Mater. Res. Soc.* **25**(8) (2000) 2.
12. J. M. Phillips, R. J. Cava, S. A. Carter, J. Kwo, S. Y. Hou, J. J. Krajewski, J. H. Marshall, W. F. Peck Jr. and D. H. Rapkine, *Appl. Phys. Lett.* **67** (1995) 2246.
13. Y. Meng, X. Yang, H. Chen, J. Shen, Y. Jiang, Z. Zhang and Z. Hua, *J. Vac. Sci. Technol. A* **20** (2002) 288.
14. Y. Yoshida, T. A. Gessert, C. L. Perkins and T. J. Coutts, *J. Vac. Sci. Technol. A* **21** (2003) 1092.
15. Y. Yoshida, D. M. Wood, T. A. Gessert and T. J. Coutts, *Appl. Phys. Lett.* **84** (2004) 2097.
16. D. Bérardan, E. Guilmeau, A. Maignan and B. Raveau, *J. Appl. Phys.* **104** (2008) 064918.
17. M. Ohtaki, D. Ogura, K. Eguchi and H. Arai, *J. Mater. Chem.* **4** (1994) 653.
18. H. Ohta, W.-S. Seo and K. Koumoto, *J. Am. Ceram. Soc.* **79** (1996) 2193.
19. M. Kazeoka, H. Hiramatsu, W.-S. Seo and K. Koumoto, *J. Mater. Res.* **13** (1998) 523.
20. Y. Masuda, M. Ohta, W.-S. Seo, W. Pitschke and K. Koumoto, *J. Solid State Chem.* **150** (2000) 221.

21. J. H. W. De Wit, J. Van Der Bom and J. F. De Groot, *J. Solid State Chem.* **25** (1978) 101.
22. J. P. Perdew, J. A. Chevary, S. H. Vosko, K. A. Jackson, M. R. Pederson, D. J. Singh and C. Fiolhais, *Phys. Rev. B* **46** (1992) 6671.
23. M. Peterson, F. Wanger, L. Hufnagel, M. Scheffler, P. Blaha and K. Schwarz, *Comput. Phys. Commun.* **126** (2000) 294.
24. P. Blaha, K. Schwarz, G. Madsen, D. Kvasnicka and J. Luitz, *Inst. f. Materials Chemistry*, TU Vienna, <http://www.wien2k.at/>.
25. G. K. H. Madsen and D. J. Singh, *Comput. Phys. Commun.* **175** (2006) 67.
26. T. J. Scheidemantel, C. Ambrosch-Draxl, T. Thonhauser, J. V. Badding and J. O. Sofo, *Phys. Rev. B* **68** (2003) 125210.
27. S. Zh. Karazhanov, P. Ravindran, P. Vajeeston, A. Ulyashin, T. G. Finstad and H. Fjellvåg, *Phys. Rev. B* **76** (2007) 075129.
28. Bilbao crystallographic server: The crystallographic site at the Condensed Matter Physics Dept. of the University of the Basque Country, <http://www.cryst.ehu.es/>.
29. J. E. Medvedeva, *Phys. Rev. Lett.* **97** (2006) 086401.
30. G. B. González, J. B. Cohen, J. H. Hwang, T. O. Mason, J. P. Hodges and J. D. Jorgensen, *J. Appl. Phys.* **89** (2001) 2550; *Handbook of Chemistry and Physics*, 85th edn., ed. D. R. Lide (CRC Press, Boca Raton, FL, 2004).
31. H. Odaka, S. Iwata, N. Taga, S. Ohnishi, Y. Kaneta and Y. Shigesato, *Jpn. J. Appl. Phys.* **36** (1997) 5551.
32. O. N. Mryasov and A. J. Freeman, *Phys. Rev. B* **64** (2001) 233111.
33. A. Walsh, J. L. F. Da Silva, S.-H. Wei, C. Körber, A. Klein, L. F. J. Piper, A. DeMasi, K. E. Smith, G. Panaccione, P. Torelli, D. J. Payne, A. Bourlange and R. G. Egdell, *Phys. Rev. Lett.* **100** (2008) 167402.
34. I. Hamberg, C. G. Granqvist, K. F. Berggren, B. E. Sernelius and L. Engström, *Phys. Rev. B* **30** (1984) 3240.
35. S. H. Brewer and S. Franzen, *Chem. Phys.* **300** (2004) 285.
36. H. Tetsuka, Y. J. Shan, K. Tezuka and H. Imoto, *Solid State Commun.* **137** (2006) 345.
37. J. E. Medvedeva and A. J. Freeman, *Europhys. Lett.* **69** (2005) 583.
38. T. L. Barr and Y. L. Liu, *J. Phys. Chem. Solids* **50** (1989) 657.